Int. J. Electrochem. Sci., 15 **(2020)** 177 – 187, doi: 10.20964/2020.01.29

International Journal of
ELECTROCHEMICAL
SCIENCE
www.electrochemsci.org

Fabrication of a Superhydrophobic Polypropylene Coating on Magnesium Alloy with Improved Corrosion Resistance

Shengjian Zhang[1,2,3], *Duanlin Cao*[1,*], *Likun Xu*[2], *Zhifeng Lin*[2], *Rongqian Meng*[1]

[1] Department of Chemistry and Chemical Engineering, North University of China, Taiyuan 030008, P. R. China
[2] State key laboratory for marine corrosion and protection, Luoyang ship material research institute, Qingdao 266235, P. R. China
[3] Department of Chemistry and Chemical Engineering, Taiyuan Institute of Technology, Taiyuan 030008, P. R. China
[*]E-mail: cdl@nuc.edu.com

Received: 5 September 2019 / *Accepted:* 25 October 2019 / *Published:* 30 November 2019

In this study, a superhydrophobic polypropylene coating was deposited on the surface of AZ31 magnesium alloy in order to improve its corrosion resistance. The substrate surface was characterized by scanning electron microscopy and X-ray photoelectron spectroscopy. The surface showed a micro-rough structure with a water contact angle of 153°. The corrosion protection performance of the coating was evaluated by potentiodynamic curves, electrochemical impedance spectroscopy and immersion testing. The results showed that the superhydrophobic coating significantly improved the corrosion resistance and self-cleaning properties of magnesium alloys.

Keywords: AZ31 magnesium alloy; polypropylene; superhydrophobicity; corrosion

1. INTRODUCTION

Magnesium (Mg) alloys as the lightest engineering material have attracted increasing attention in the fields of automobiles, biological materials and aircraft due to their high specific strength, machinability and excellent electromagnetic shielding properties [1-5]. However, Mg is highly corrosive which may impair the physical properties and thus severely limit the application of Mg alloys [9-10]. Thus, there is a practical need to deposit a protective coating on Mg alloys operating in corrosive environments. In recent years, many coatings have been developed to improve the corrosion resistance of Mg alloys, such as chromate conversion coatings [6-8], metallic coatings [11-12], micro-arc oxidation coatings [13-15] and organic coatings [16]. However, these coatings may have micropores and cracks through which the corrosive medium can reach the surface of the substrate,

resulting in a reduction in corrosion resistance. This problem can be solved by preparing a water-repellent surface that can prevent the penetration of corrosive medium into the Mg alloy matrix.

Superhydrophobic surfaces have found many industrial applications such as antifouling paints [17], anti-icing coatings [18-19], water-in-oil emulsion separation [20], reduced fluid resistances [21] and self-cleaning coatings [22-23] due to their high water contact angles (CA > 150◦), and it is essential for them to have rough surface and low surface energy. Over the past decades, many techniques have been applied to fabricate superhydrophobic coatings on the surface of Mg alloys, including hydrothermal synthesis [24], electrodeposition [25], chemical etching [26-28] and electroless plating [29-30]. Polypropylene (PP) is an environmentally friendly and non-toxic polymer with excellent corrosion and water resistance, as it is intrinsically hydrophobic with a low surface energy of 3×10^{-2} N m^{-1} [31], which make it useful in the manufacture of superhydrophobic surfaces [31-34].

Polypropylene grafted maleic anhydride (PP-g-MAH) was synthesized by grafting maleic anhydride (MAH) with anhydride groups onto PP and then used as the compatibilizer for improving the adhesion between PP and the MgO layer. A simple and effective method was proposed in this study for preparing superhydrophobic coatings. A MgO layer was deposited on the surface of Mg alloys by anodic oxidation (MgO/Mg), and then 1% PP-g-MAH and 1% PP were used to construct nanometers on the surface of MgO. The results showed that the superhydrophobic surface significantly improved the corrosion resistance of Mg alloys in 3.5% NaCl solution.

2. EXPERIMENTAL

2.1. Materials

Commercial AZ31 Mg alloy plates were cut into pieces of 20×30×2.5 mm and used as the substrates. PP-g-MAH with a 1.5% grafting ratio and isotactic PP particles were purchased from Jinkang New Material Technology Co. LTD (China). NaOH and $NaSiO_3{\cdot}H_2O$ were of analytical grade. All regents were used as received without further purification.

2.2 Fabrication of the superhydrophobic surface

AZ31 Mg alloy samples were polished with 800 and 1500# emery paper and then ultrasonically degreased in ethanol to obtain a smooth surface. The anodic oxidizing electrolyte was composed of 120 g/L NaOH and 80 g/L $NaSiO_3{\cdot}H_2O$. Anodization was carried out at 10 V with a duration time of 20 min, and the polished AZ31 substrate was used as the anode and a lead plate was used as the cathode. The oxidized Mg samples (MgO/Mg) were rinsed with deionized water and dried at ambient temperature. Then, 1% PP and 1% PP-g-MAH were dissolved in xylene solution (1 g of PP or PP-g-MAH and 98 g of xylene), and then heated to 125 ° C in a sealed oil bath until PP and PP-g-MAH were completely dissolved. The MgO/Mg samples were dip coated in the prepared solution for 3 min, dried in ambient air for 10 min, aged at 100° C in oven for 10 min and then air cooled to obtain PP-MgO/Mg samples.

2.3 Characterizations

The morphology was observed using a field emission scanning electron microscope (FSEM, JSM-7200F, Japan) coupled with an energy disperse X-ray spectrometer (EDS). The static water contact angles of surfaces were measured by an optical contact angle meter (Model Powereach JC2000D, China) at ambient temperature using a drop of deionized water. The CA values at three different positions of the substrate were measured and the average was calculated for analysis.

Electrochemical impedance spectroscopy (EIS) and potentiodynamic polarization were performed on a CHI model 660E electrochemical work station (Shanghai Chenhua, China) equipped with a standard three-electrode system, where a saturated calomel electrode was used as the reference electrode, a platinum plate was used as the counter electrode, and the sample was used as the working electrode in 3.5 wt% NaCl aqueous solution. Potentiodynamic polarization curves were obtained at a scanning rate of 1 mV s^{-1} from -2 V to -1 V (vs SCE). EIS measurements were conducted in the frequency range from 10^5 Hz to 10^{-2} Hz at an open circuit potential with a sinusoidal signal of 5 mV. All measurements were performed at room temperature. In order to further evaluate the long-term corrosion resistance of PP-MgO/Mg, samples were immersed in 3.5 wt% NaCl solution for EIS measurement every 12h.

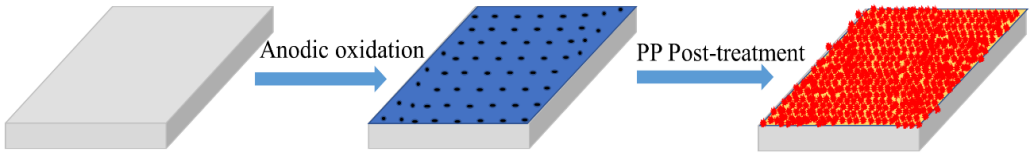

Scheme 1. Schematic of the fabrication of polypropylene on the surface of AZ31 Mg alloy.

3. RESULTS AND DISCUSSION

3.1 Wettability of the super-hydrophobic surface

The wettability of PP-MgO/Mg before and after modification is indicated by the CA on the surface. As shown in Fig. 1, surface modification results in a substantial change in hydrophobicity of the coating. The water droplets are almost spherical on the surface of PP-MgO/Mg, which can reduce the surface energy. The CA (153°) is much higher than that on the Mg surface (42°), indicating a superhydrophobic surface. Before modification, the CA of MgO/Mg is about 19° and the water droplets can quickly spread on the surface. The coating on the surface of the Mg alloy is superhydrophobic and thus the water droplets can move easily even when the sample is only slightly tilted, which is mainly due to the micro- and nano-scale binary structures that can trap enough air and the low surface energy of the PP layer that can prevent the penetration of water droplets [35].

Figure 1. The CA images of (a) Mg (b) MgO/Mg and (c) PP-MgO/Mg samples

3.2 Stability of the PP-MgO/Mg superhydrophobic coating

Fig. 2 shows the relationship between immersion time and CA of the superhydrophobic coating in 3.5 wt% NaCl solution. It is seen that the CA decreases slowly within the first 20 min but more rapidly at 20-60 min. Notably, the CA is still as high as 150° after immersion for 20 min, and it is decreased to 130° as the immersion time is extended to 120 min. However, no significant changes are observed in the surface structure of the coating, indicating that the coating can maintain a large CA in 3.5 wt% NaCl solution for a long period of time.

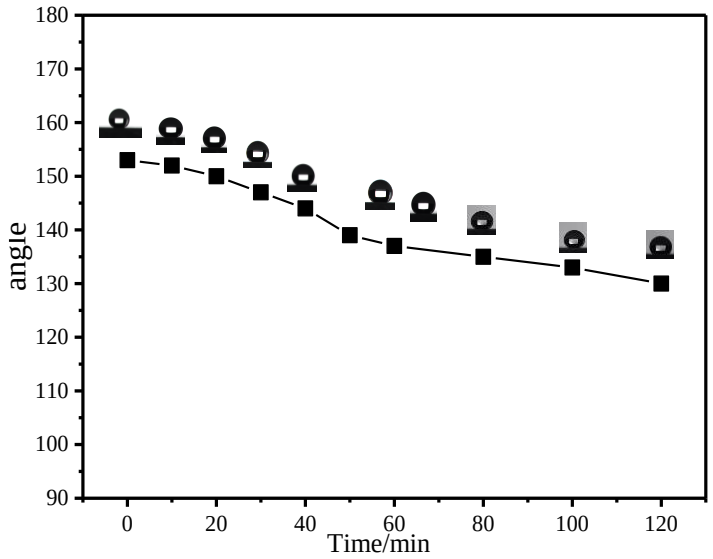

Figure 2. The relationship of CA with immersion time in 3.5 wt% NaCl solution.

3.3 Surface properties of composite coatings

Fig. 3 shows the surface and cross-sectional morphologies of PP-MgO/Mg. Fig. 3a shows that the surface of Mg alloy is almost completely covered by PP and PP-g-MAH, which are connected to each other to form a continuous network structure with microspheres on the surface of Mg alloy. These microspheres show a rough porous structure, making it possible to capture more air in the porous

structure and reduce the contact area. According to the Cassie–Baxter model, the micro-nano structure can improve the hydrophobic properties of the sample [37-38]. The diameters of pores are often tens of nanometers. Fig. 3c shows that both PP and PP-g-MAH layers are about 18-26 μm thick. The EDX analysis results show that the layer is composed of 86.87% C, 7.91% O, 4.51% Mg and 0.71% Si.

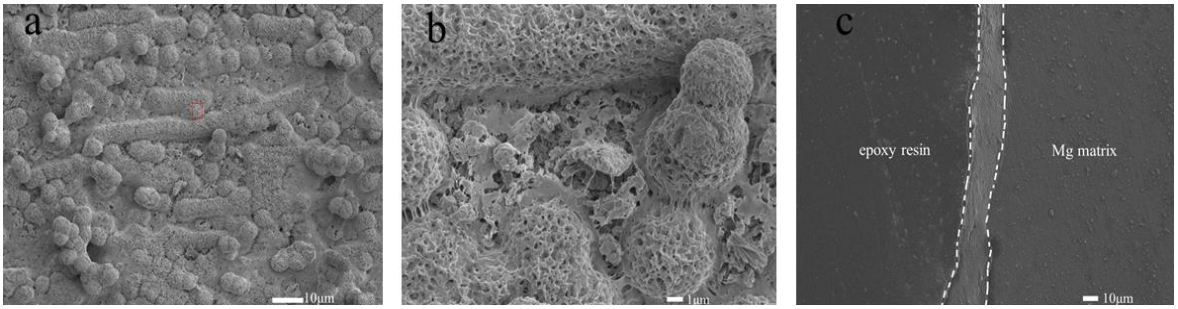

Figure 3. SEM images of PP-MgO/Mg samples. (a-b) surface and (c) cross-section morphology

3.4. Corrosion resistance of superhydrophobic coatings

The potentiodynamic polarization curves of Mg, MgO/Mg and PP-MgO/Mg in 3.5 wt% NaCl solution are shown in Fig. 4, and their corrosion potential (*E*corr) and corrosion current density (*i*corr) derived from Fig. 3 are summarized in Table 1.

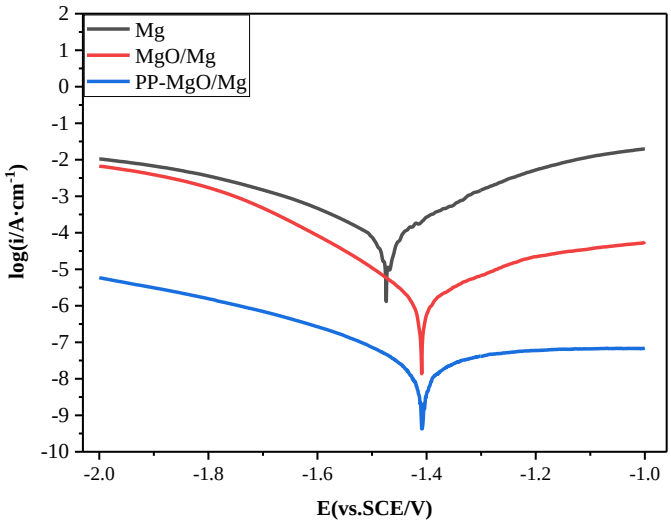

Figure 4. Potentiodynamic curves of (a) Mg, (b) MgO/Mg and (c) PP-MgO/Mg in 3.5% wt NaCl solution.

It shows that *E*corr is increased from -1.474 V for Mg to −1.409 V for MgO/Mg and to −1.407 V for PP-MgO/Mg. Compared with MgO/Mg (1.678×10^{-6}A cm^{-2}), the *i*corr of PP-MgO/Mg is increased by two orders of magnitude (1.626×10^{-8}A cm^{-2}), because the MgO layer is imperfect and could not provide sufficient protection for AZ31 and the transfer rate of Cl^- is low due to the presence

of PP superhydrophobic coating between the Mg alloy matrix and the corrosive medium. The polarization curves of MgO/Mg and PP-MgO/Mg samples are very similar, indicating that the PP film acts only as a physical barrier on the surface without changing the electrode reaction kinetics of both cathode and anode [38-39].

The experimental results show that the as-prepared PP superhydrophobic layer is very effective in improving the corrosion resistance of AZ31 and maintaining the damping capacity [40-41]. This is because the PP superhydrophobic coating can capture more air to prevent the contact of the corrosive medium with the Mg alloy, and it can also form an effective barrier to moisture and oxygen [42-43].

Table 1. Potentiodynamic resistances of Mg, MgO/Mg and PP-MgO/MgO in 3.5% wt NaCl solution.

Samples	I_{corr} (mA·cm^{-2})	E_{corr} (mV)	-βc(mV·dec-1)	βa(mV·dec^{-1})
Mg	0.0375	-1474	246	426
MgO/Mg	0.0036	-1409	265	629
PP-MgO/Mg	4.27×10^{-5}	-1407	121	228

Fig. 5 shows the EIS spectra of different samples immersed in 3.5 wt% NaCl solution for 30 min, and Fig. 6 and Table 2 show their equivalent circuits and EIS simulation results. Two time constants can be found in the Bode plots of the PP-MgO/Mg coating in the high frequency region (10^3-10^5). The capacitive impedance loop is attributed to the presence of the PP superhydrophobic coating, and another capacitive impedance loop in the middle frequency region (10^{-1}-10^3) is caused by MgO on the surface of Mg alloy. At 0.01 Hz, the |Z| value of PP-MgO/Mg is 2.93×10^7 Ω·cm^2, which is about four orders of magnitude higher than that of MgO/Mg. However, the |Z| value of Mg alloys is only a few dozen. PP-MgO/Mg has a wider phase angle, indicating that the PP superhydrophobic coating can effectively prevent the corrosion medium from entering the matrix.

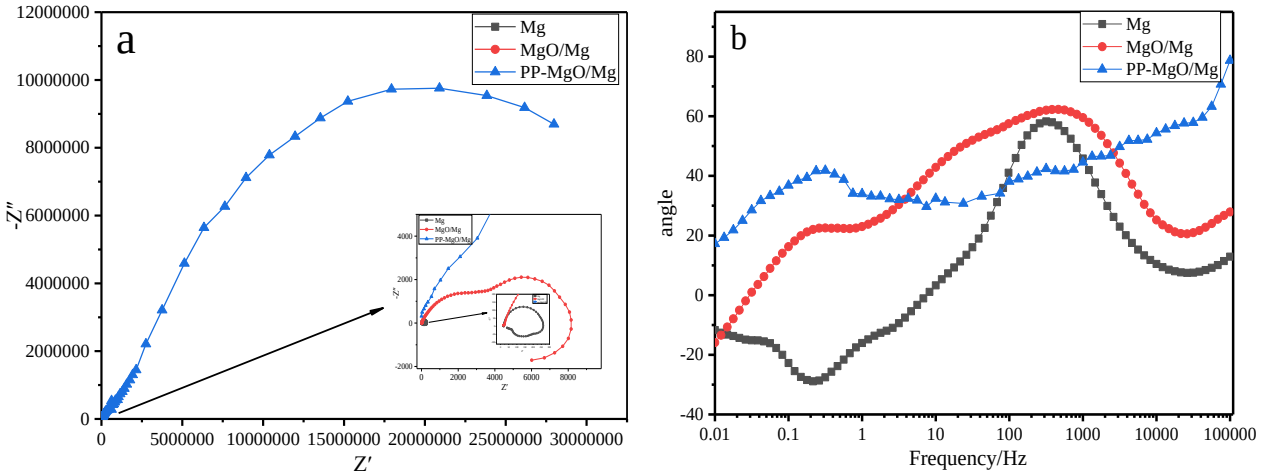

Figure 5. EIS for samples immersed in 3.5 wt% NaCl solution: (a) Nyquist plots and (b) Bode plots of phase angle vs. frequency.

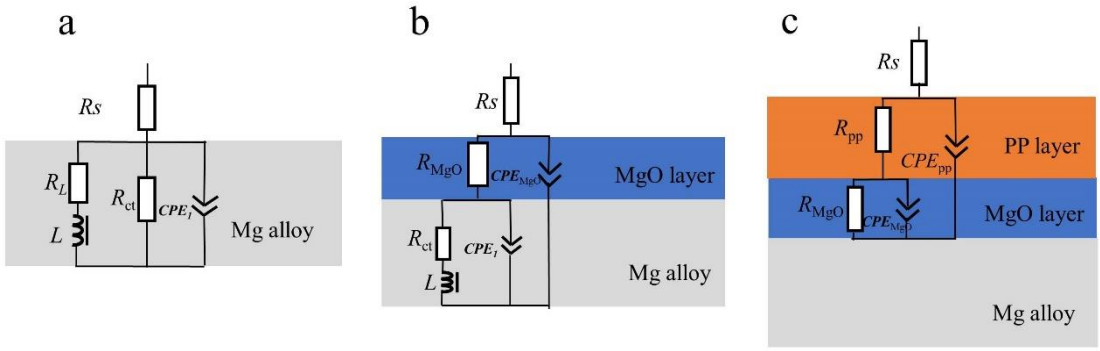

Figure 6. Equivalent circuits for samples in 3.5 wt% NaCl solution. (a) Mg, (b) MgO/Mg and (c) PP-MgO/Mg

Table 2. EIS simulation results for different samples immersed in 3.5 wt% NaCl solution.

Samples	*R*s Ωcm^2	*CPE*pp μFcm^{-2}	n_1	R_{PP} Ωcm^2	CPE_{MgO} μFcm^{-2}	n_2	R_{MgO} Ωcm^2	CPE_{ct} μFcm^{-2}	n_3	R_{ct} Ωcm^2	*L*
PP-MgO/Mg	15.81	3.5×10^{-8}	0.591	1.47×10^{6}	6.33×10^{-8}	0.807	2.81×10^{7}	…	…	…	…
MgO/Mg	18.37				1.56×10^{-5}	0.766	2076	2.41×10^{-4}	0.281	3989	6.88×10^{-4}
Mg	18.42							6.21×10^{-6}	0.997	168.7	62.68

3.5 Durability of superhydrophobic coatings

Fig. 7 shows the electrochemical impedance spectra of PP-MgO/Mg sample at different times. The equivalent circuits are shown in Fig. 8 and fitted parameters are summarized in Table 3. The Bode plots of phase angle vs. frequency show that the corrosion of PP-MgO/Mg in 3.5 wt% NaCl solution can be divided into three stages. The impedance is very high in the first stage (1-84 h). After immersion in 3.5 wt% NaCl solution for 12 h, PP-MgO/Mg samples show high impedance ($2.04\times10^{7}\Omega\cdot cm^2$) in the low frequency region, because the hydrophobic nature of the PP film layer makes it extremely difficult for the corrosive medium to enter the coating. After immersion for 24 h, the impedance is decreased at a faster rate to 4.87×10^{6} $\Omega\cdot cm^2$. As the immersion time is further extended, the capacitance loop in the intermediate frequency region shifts to higher frequency region. This is because the blocking ability of the PP layer decreases, so that it is easier for the corrosive medium to enter the PP layer. Three time constants are obtained in the second stage (84-252 h), indicating that the corrosive medium has reached the oxide layer. The time constant corresponding to the low frequency band (10^{-2}-10^{-1}) is attributed to the presence of the inner barrier layer. In the final stage (>264 h), the inductance loop appears in the low frequency phase angle and the impedance drops to several hundred $\Omega\cdot cm^2$ at 0.01 Hz, indicating that the corrosive medium contacts the surface of the Mg substrate to dissolve the Mg matrix, causing pitting corrosion damage [44].

The equivalent circuits shown in Fig. 8 are used to explain the EIS of PP-MgO/Mg immersed for different times, and the corresponding fitting results are summarized in Table 3, where *R*s is the solution resistance, R_{PP} and *CPE*pp are the resistance of the PP film layer and the corresponding capacitive components, R_{MgO} and CPE_{MgO} are the resistance of the MgO layer and the corresponding capacitive components, R_{ct} and CPE_{ct} are the charge transfer resistance and capacitance components of

the Mg alloy interface, and *L* is an inductive component of the equivalent circuit, respectively. The *R*pp value is 2.01×10^7 Ω·cm^2 after immersion in the solution for 1 h and decreased by about an order of magnitude to 2.87×10^6 Ω·cm^2 after immersion for 84 h. The R_{MgO} value is also decreased, implying a decrease in the ability of the PP layer to block corrosive medium [38]. In the final stage of immersion, the electrolyte reaches the surface of the Mg alloy matrix, so that the Mg alloy is dissolved to form $Mg(OH)_2$ and, as a consequence, the PP coating will completely lose its protective effect on the Mg alloy matrix [44].

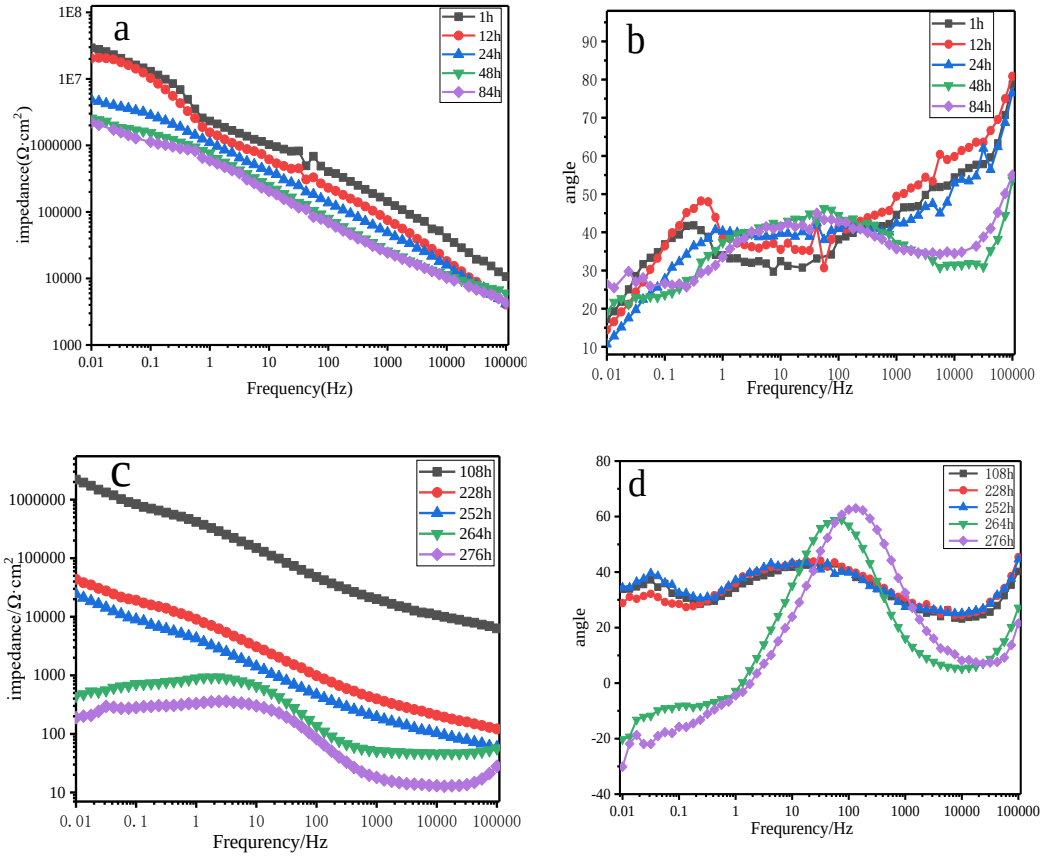

Figure 7. EIS of PP-MgO/Mg immersed in 3.5 wt% NaCl solution: (a, c) Nyquist plots and (b, d) Bode plots of phase angle vs. frequency.

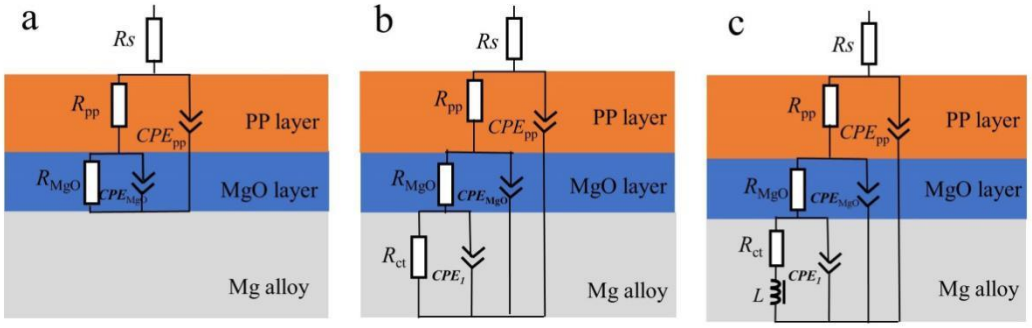

Figure 8. Equivalent circuits for the PP-MgO/Mg immersed in 3.5 wt% NaCl solution. (a) 1-84 h, (b) 108-252 h and (c) 264-276 h

Table 3. EIS simulation results for PP-MgO/Mg immersed in 3.5 wt% NaCl solution.

Time/ h	*R*s Ωcm^2	*CPE*pp μFcm^{-2}	n_1	R_{PP} Ωcm^2	CPE_{MgO} μFcm^{-2}	n_2	R_{MgO} Ωcm^2	CPE_{ct} μFcm^{-2}	n_3	R_{ct} Ωcm^2	*L*
1h	15.81	3.5×10^{-8}	0.591	1.47×10^{6}	6.33×10^{-8}	0.807	2.81×10^{7}	…	…	…	…
12h	17.78	1.33×10^{-7}		1.34×10^{5}	1.46×10^{-7}	0.521	1.27×10^{7}	…	…	…	…
24h	16.47	3.47×10^{-10}	1	6087	3.41×10^{-7}	0.472	1.363×10^{7}	…	…	…	…
48h	18.45	1.76×10^{-10}		6455	4.46×10^{-7}	0.525	3.013×10^{6}	…	…	…	…
84h	16.82	2.51×10^{-10}		5168	6.11×10^{-7}	0.493	2.866×10^{6}	…	…	…	…
108h	18.77	4.25×10^{-9}	0.757	9931	5.51×10^{-6}	0.889	2.74×10^{6}	6.53×10^{-7}	0.551	8.96×10^{5}	…
228h	29.64	4.52×10^{-5}	0.379	698.4	3.28×10^{-6}	0.782	5.2×10^{4}	2.8×10^{-8}	0.205	8.31×10^{4}	…
252h	26.33	8.67×10^{-8}		6.543	1.28×10^{-4}	0.545	3383	2.5×10^{-4}	0.577	1.27×10^{4}	…
264h	16.06	1.77×10^{-5}	0.954	0.05872	1.38×10^{-9}	0.012	332	2.09×10^{-3}	0.81	126.1	1314
276h	17.64	2.34×10^{-5}	0.972	1.24×10^{-6}	8.22×10^{-10}	0.029	$4.31*10^{5}$	3.14×10^{-3}	0.83	204	2828

3.6 Hydrophobic and self-cleaning effect of superhydrophobic coatings

Fig. 9 shows the photos of the surfaces of different samples. It can be seen that the blue water droplets can wet Mg and MgO/Mg and spread rapidly on the surface; while PP treatment makes the sample more hydrophobic and thus the blue water droplets remain spherical on the surface.

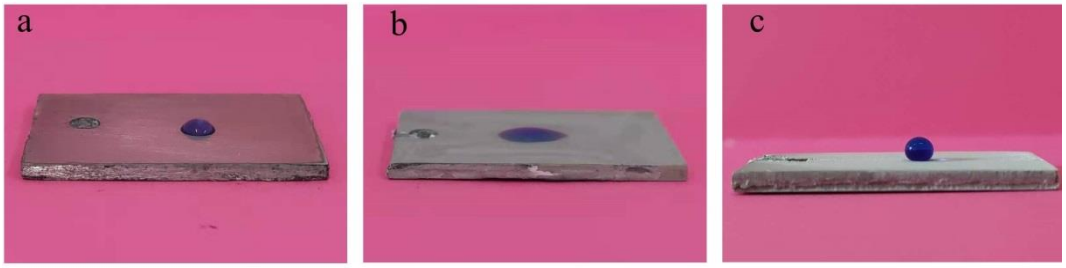

Figure 9. Photos of water droplets on the surface. (a) Mg, (b) MgO/Mg and (c) PP-MgO/Mg samples

Figure 10. Self-cleaning behavior on the surface of super-hydrophobic coatings.

Multi-walled carbon nanotube (CNT) powders are deliberately dispersed on the sample surface as stains (Fig. 10a), and then a water droplet is dropped through a plastic dropper onto the upper side of the sample surface (Fig. 10b). Clearly, the water droplet falling on the superhydrophobic surface can

roll up and down freely, resulting in the removal of multi-walled CNT powders. The results show that the superhydrophobic Mg surface has a self-cleaning effect, which is similar to lotus leaves. This is mainly attributed to the synergistic effect of the low surface energy and certain roughness [45].

4. CONCLUSIONS

Surface modification of Mg alloys with PP results in formation of a superhydrophobic coating with a CA of 153°. The sample exhibits excellent corrosion resistance and low corrosion current density due to the barrier and blocking ability of the PP layer. The superhydrophobic surface also has a self-cleaning ability.

References

1. M. Gzyl, R. Pesci, A. Rosochowski, S. Boczkal, L. Olejnik,. *J. Mater. Sci.*, 50(2015) 2532.
2. C.L. Wang, G. H. Wu, E. J. Lavernia, W.J. Ding. *J. Mater. Sci.*, 52(2017) 1831.
3. N. D. Nam, W. C. Kim, J. G. Kim, K. S. Shin, H. C. Jung. *Corros. Sci.*. 51(2009) 2942.
4. H. Altun, S. Sen. *Mater. Des.*, 25(2004) 637.
5. J. Liang, B.G. Guo, J. Tian, H.W.vLiu, J.F. Zhou, T. Xu. *Appl. Surf. Sci.*, 252(2005) 345.
6. S. Pommiers, J. Frayret, A. Castetbon, M.P. Gautier. *Corros. Sci.*,84(2014)135.
7. C.D. Ding, Y. Liu, M.D. Wang, T. Wang , J.J. Fu. *J. Mater. Chem. A*, 4(2016)8041.
8. T.H. Tran , A. Vimalanandan , G. Genchev , J. Fickert , K. Landfester , D. Crespy , M. Rohwerder. *Adv. Mater.*, 27(2015)3825.
9. Z.W. Song, Z. H. Xie, B.N. Hu, X.M. He, X.Y. Zhang. *J. Alloys Compd.*, 623(2015)274.
10. F. Tuchscheerer, L. Krüger. *J. Mater. Sci.*, 50(2015) 5104.
11. Z.C. Shao, F.F. Zhang, Z.Q. Cai, R. Hu. *Anti-Corros. Methods Mater.*, 64(2017)162.
12. H.Y. Yang, X.W. Guo, X.B. Chen, N. Birbilis. *Corros. Sci.*,79(2014)41.
13. S. Durdu, M. Usta. Appl. *Surf. Sci.*, 261(2012)774.
14. R.F. Zhang. *Corros. Sci.*,52(2012)1285.
15. R.F.Zhang, S.F.Zhang, Y.L.Shen, L.H.Zhang, T.Z.Liu, Y.Q.Zhang, S.B.Guo. *Appl. Surf. Sci.*, 258(2012)6602.
16. X.Y. Lu, X.G. Feng, Y. Zuo, C.B. Zheng, S. Lu, L. Xu. *Surf. Coat. Technol.*, 270(2015)227.
17. M. Ferrari, A. Benedetti, E. Santini, F. Ravera, L. Liggieri, E. Guzman, F. Cirisano. *Colloids Surf., A*, 480(2015)369.
18. R.J. Liao, Z.P. Zuo, C. Guo, Y. Yuan, A.Y. Zhuang. *Appl. Surf. Sci.*, 317(2014)701.
19. Y. Le, B, Dale, F, Akisik, K. Koons, C, Lin. *Langmuir*, 29(2013)8482.
20. Y.Z. Zhu, D. Wang, L. Jiang , J. Jin. *NPG Asia Mater.*, 6(2014) e11.
21. Y. Kwon, N. Patankar, J. Choi, J. Lee. *Langmuir*, 25(2009)6129.
22. S.S. Latthe, P. Sudhagar, A. Devadoss, A. M. Kumar, S. Liu,c C. Terashima, Kazuya Nakata, A. Fujishima. *J. Mater. Chem. A*, 3(2015)14263.
23. A.K. Sasmal, C. Mondal, A. K. Sinha, S. S. Gauri, J.Pal, T.Aditya, M.Ganguly, S. Dey, T. Pal. *ACS Appl. Mater. Interfaces*, 6(2014)22034.
24. L. Feng, Y. Zhu, J. Wang, X. Shi. *Appl. Surf. Sci.* 422 (2017) 566.
25. Q. Liu, D. Chen, Z. Kang. *ACS Appl. Mater. Interfaces*, 7 (2015) 1859.
26. H.F.Gao, H.Q.Tan, J.Li, Y.Q.Wang, J.Q.Xun. *Surf. Eng.*,28(2012)387.
27. B.T. Qian, Z.Q. Shen. *Langmuir*, 21(2005)9007.
28. Y. F. Luo, H.Y. Lang, J. Liang, G.S. Peng, Y.H. Fan, M.L. Zhang, Z.Q. Yuan, H. Chen. *Adv. Mater.*

Res., (2011)239.
29. J. Yuan, J.H. Wang, K.L. Zhang, W.B. Hu. *RSC Adv.*, 7(2017)28909.
30. I. Daisuke, S. Masatsugu, A. J. Nanosci. *Nanotechnol.*, 14(2014)7611.
31. Himma, Nurul , A. Wardani , I. G. Wenten . *Mater. Res. Express*, 4(2017).
32. W.Y. Liu, Y.T. Luo, L.Y. Sun, R.M. Wu, H.Y. Jiang, Y.J. Liu. *Appl. Surf. Sci.*, 264(2013)872.
33. T. Zhu, C. Cai, J. Guo, R. Wang, N. Zhao, J. Xu. *ACS Appl. Mater. Interfaces*, 9(2017)10224.
34. C.B.Contreras, G. Chagas, M. C.Strumia, D. E.Weibel. *Appl. Surf. Sci.*, 307(2014)234.
35. Q. Chu, J. Liang, J, Hao. *Colloids Surf., A*, 443(2014)118.
36. I. Hejazi, B. Hajalizadeh, J. Seyfi, G.M.M. Sadeghi, S.H. Jafari, H. AliKhonakdar. *Appl. Surf. Sci.*,293(2014)116.
37. D. Jiang, H. Zhou, S. Wan, G.Y. Cai, Z.H. Dong. *Surf. Coat. Technol.*, 339(2018)155.
38. M.A. Chen, S.Y. Liu, J.M. Li, N. Cheng, X.M. Zhang. *Surf. Coat. Technol.*, 232(2013)674.
39. W.J. van Ooij, D. Zhu, M. Stacy, A. Seth, T. Mugada, J. Gandhi, P. Puomi, *Tsinghua. Sci. Technol.*, 10 (2005) 639.
40. T. Ishizaki, Y. Masuda, M. Sakamoto, *Langmuir,* 27 (2011) 4780.
41. L. Zhao, Q. Liu, R. Gao, J. Wang, W.L. Yang, L.H. Liu, *Corros. Sci.*, 80(2014)177.
42. T. Ishizaki, N. Saito, *Langmuir,* 26 (2010) 9749.
43. H.Q. Liu, S. Szunerits, W.G. Xu, R. Boukherroub, *ACS Appl. Mater. Interfaces*, 1(2009) 1150.
44. M.A. Chen, C. Xiao, J.M. Li. *Trans. IMF*, 91(2013)80.
45. Y. Wu, Y.Z. Shen, J. Tao, Z.R. He, Y.H. Xie, H.F. Chen, M.M Jin, W.Q. Hou. *New J. Chem.*, 42(2018)18208.